

Temperature-dependent quantum pair potentials and their application to dense partially ionized hydrogen plasmas

A.V. Filinov¹, V.O. Golubnychiy², M. Bonitz¹, W. Ebeling³, and J.W. Dufty⁴

¹*Institut für Theoretische Physik und Astrophysik,*

Christian-Albrechts-Universität Kiel, Leibnizstr. 15, D-24098 Kiel, Germany

²*Fachbereich Physik, Universität Rostock, Universitätsplatz 3, D-18051 Rostock, Germany*

³*Institut für Physik, Humboldt-Universität Berlin, Invalidenstrasse 110 D-10115 Berlin and*

⁴*University of Florida, Department of Physics, PO Box 118440, Gainesville FL 32611-8440*

Extending our previous work [1] we present a detailed discussion of accuracy and practical applications of finite-temperature pseudopotentials for two-component Coulomb systems. Different pseudopotentials are discussed: i) the diagonal Kelbg potential, ii) the off-diagonal Kelbg potential iii) the *improved* diagonal Kelbg potential, iv) an effective potential obtained with the Feynman-Kleinert variational principle v) the “exact” quantum pair potential derived from the two-particle density matrix. For the *improved* diagonal Kelbg potential a simple temperature dependent fit is derived which accurately reproduces the “exact” pair potential in the whole temperature range. The derived pseudopotentials are then used in path integral Monte Carlo (PIMC) and molecular dynamics (MD) simulations to obtain thermodynamical properties of strongly coupled hydrogen. It is demonstrated that classical MD simulations with spin-dependent interaction potentials for the electrons allow for an accurate description of the internal energy of hydrogen in the difficult regime of partial ionization down to the temperatures of about 60 000 K. Finally, we point out an interesting relation between the quantum potentials and effective potentials used in density functional theory.

I. INTRODUCTION

In recent years there is growing interest in the properties of dense *quantum* plasmas, particularly in astrophysics, laser plasmas, and condensed matter, see Refs. [2, 3, 4, 5, 6, 7] for an overview. In particular, the thermodynamic properties of hot dense plasmas are essential for the description of plasmas generated by strong lasers [6]. Further, among the phenomena of current interest are the high-pressure compressibility of deuterium [8], metallization of hydrogen [9] and the hypothetical plasma phase transition, e.g. [10, 11, 12, 13, 14, 15, 16] which occur in situations where both *interaction and quantum effects* are relevant.

While the case of strong degeneracy and the weak coupling limit have been extensively studied theoretically, e.g. within the random phase approximation, plasma properties at *intermediate coupling and degeneracy* (when $\beta\mu$ - the ratio of the potential energy to the mean kinetic energy exceeds unity), are a hot topic of the present research activity. For an overview of present day analytical methods, see e.g. Refs. [2, 3, 5, 14]. Analytical methods typically use a chemical picture where electrons, ions and bound states (atoms, molecules etc.) are treated as independent species, and the chemical composition (degree of ionization) is computed from a mass action law (non-ideal Saha equation). However, these methods are based on perturbation expansions in the coupling strength and are thus limited to regions of small coupling parameters, $\beta\mu < 1$ or $r_s < 1$ (r_s is the quantum coupling parameter, $r_s = r/a_B$). Furthermore, the mass action law becomes increasingly inaccurate in the region where the electrons are degenerate (uncertainty in the mass action constants). Also, during rapid pressure ionization around the Mott density the distinction between

free and bound particles is an open problem.

On the other hand, in the last decade, static properties (e.g. equation of state) of dense hydrogen in thermal equilibrium have been successfully investigated with “exact” quantum-statistical methods, such as path integral Monte Carlo (PIMC) [17, 18, 19, 20]. This first principle numerical technique is well suited for an accurate treatment of many-particle correlation effects in quantum systems, but unfortunately does not give dynamical characteristics of the plasma (with an exception of those obtained within the linear response theory). The alternative numerical approach for dense partially ionized plasmas (which does not have the above shortcoming) is a group of methods based upon ab initio quasi-classical molecular dynamic simulations (MD), e.g. Refs. [21, 22], when a real quantum system is projected onto a classical one where most of quantum effects are included in some effective interparticle interaction potentials, such as the ones proposed by Kelbg [25], Deutsch [26], Klakow, Toepffer and Reinhard [21] and many others, e.g. [27, 28, 29]. These potentials can be derived from the two-particle Slater sum using Morita’s method.

However, no rigorous comparison of the accuracy of these potentials has been done yet, which is one of the aims of this paper. Different quantum potentials are compared with an “exact” pair potential obtained from the two-particle density matrix. Furthermore, we introduce pair potentials including particle statistics, e.g. describing interaction between electrons in the singlet and triplet states, and use them in our MD simulations of two-component hydrogen plasmas.

This paper is organized as follows: In Section II we discuss different methods to obtain an effective quantum pair potential. In the weak coupling limit, this poten-

tial leads exactly to the off-diagonal Kelbg potential the properties of which are being discussed and compared to its commonly used diagonal approximation. We outline two methods for a direct solution of the off-diagonal two-body Bloch equation which are then used in Section III for numerical comparison with the Kelbg and improved Kelbg potentials for rigorous assessment of the accuracy of the latter. Further, in Section IV we present an analysis of the accuracy of the diagonal and off-diagonal Kelbg potentials in the PIMC simulations. Section V describes an application of the improved Kelbg potentials to classical molecular dynamics simulations of dense hydrogen. Comparing the results to those of PIMC simulations allows us to conclude that use of the improved Kelbg potential allows to significantly extend the range of applicability of classical MD to the region of partial ionization and to temperatures as low as approximately one third of the binding energy. Section VI discusses another field of potential applicability of the quantum potentials – density functional theory. Finally, Section VII concludes the paper.

II. EFFECTIVE QUANTUM PAIR POTENTIALS

In this section we discuss different possibilities to obtain effective quantum potentials describing interactions in the two-particle problem.

A. Analytical solution of two-body Bloch equation. Off-diagonal and diagonal Kelbg potential

The equilibrium pair density matrix at a given inverse temperature $\beta = 1/k_B T$ is the solution of the two-particle Bloch equation

$$\frac{\partial}{\partial \beta} \langle \mathbf{r}_i; \mathbf{r}_j; \mathbf{r}_i^0; \mathbf{r}_j^0 \rangle = -\hat{H} \langle \mathbf{r}_i; \mathbf{r}_j; \mathbf{r}_i^0; \mathbf{r}_j^0 \rangle; \quad \hat{H} = \hat{K}_i + \hat{K}_j + \hat{U}(\mathbf{r}_i; \mathbf{r}_j; \mathbf{r}_i^0; \mathbf{r}_j^0); \quad (1)$$

Numerical methods to obtain the density matrix of the Eq. (1) will be considered in Sec. II C. Here, we concentrate on the available analytical solutions in the limit of weak coupling. If the interaction is weak, the Eq. (1) can be solved by perturbation theory with the following representation for the two-particle density matrix

$$\langle \mathbf{r}_i; \mathbf{r}_j; \mathbf{r}_i^0; \mathbf{r}_j^0 \rangle = \frac{(m_i m_j)^{3/2}}{(2\pi\hbar^2)^3} \exp\left[-\frac{m_i}{2\hbar^2}(\mathbf{r}_i - \mathbf{r}_j^0)^2\right] \exp\left[-\frac{m_j}{2\hbar^2}(\mathbf{r}_i - \mathbf{r}_j^0)^2\right] \exp[-\beta U(\mathbf{r}_i; \mathbf{r}_j); \quad (2)$$

where i, j are particle indices, $\langle \mathbf{r}_i; \mathbf{r}_j; \mathbf{r}_i^0; \mathbf{r}_j^0 \rangle$, and $\langle \mathbf{r}_i; \mathbf{r}_j; \mathbf{r}_i^0; \mathbf{r}_j^0 \rangle$ is the off-diagonal two-particle

effective potential. In the following we will consider application of this result to Coulomb systems. As a result of first-order perturbation theory we get explicitly

$$\langle \mathbf{r}_i; \mathbf{r}_j; \mathbf{r}_i^0; \mathbf{r}_j^0 \rangle = \frac{Q_i Q_j}{(2\pi\hbar^2)^3} \int_0^\beta \frac{d\tau}{d_{ij}(\tau)} \exp\left[-\frac{d_{ij}(\tau) - d_{ij}(0)}{2\hbar^2} U(\mathbf{r}_i; \mathbf{r}_j)\right]; \quad (3)$$

where $d_{ij}(\tau) = \frac{1}{2} \mathbf{r}_{ij} + (1-\tau) \mathbf{r}_{ij}^0$, $\text{erf}(\mathbf{x})$ is the error function, $\text{erf}(\mathbf{x}) = \frac{2}{\sqrt{\pi}} \int_0^{\mathbf{x}} dt e^{-t^2}$, and $\frac{1}{d_{ij}} = \frac{1}{2} \frac{1}{d_{ij}} + \frac{1}{2} \frac{1}{d_{ij}}$. The diagonal element ($\mathbf{r}_{ij}^0 = \mathbf{r}_{ij}$) of (3) is the potential derived by Kelbg and his coworkers [4, 25]

$$\langle \mathbf{x}_{ij} \rangle = \frac{Q_i Q_j}{(2\pi\hbar^2)^3} \int_0^\beta \frac{d\tau}{d_{ij}(\tau)} \exp\left[-\frac{1}{2} \mathbf{x}_{ij}^2 + \frac{1}{2} \mathbf{x}_{ij}^2 \text{erf}(\mathbf{x}_{ij})\right] \quad (4)$$

with $\mathbf{x}_{ij} = \mathbf{r}_{ij} - \mathbf{r}_{ij}^0$. The Kelbg potential is finite at zero distance reflecting that it captures the basic quantum diffraction effects and the quantum nature of two-particle interaction at small distances which prevents any divergence. From Eq. (4) it is also clear that quantum effects become dominant (and there the quantum potential deviates from the classical Coulomb potential) at distances $r_{ij} \sim \lambda_{ij}$ given by the thermal DeBroglie wavelength. We will see below that, in interacting systems, this is only a rough approximation, and at strong coupling, the expression for the quantum particle “extension” deviates strongly from λ_{ij} and needs to be generalized.

To obtain a simplified expression for the rather complex quantum potential (3) one can approximate the off-diagonal matrix elements by the diagonal ones. A first possibility is to approximate the integral over τ by the length of the interval multiplied with the integrand in the center (Mittelwertsatz) which leads to the so-called KTR-potential due to Klakow, Toepffer and Reinhard which (in the diagonal approximation) is often used in quasi-classical MD simulations [21]

$$\langle \mathbf{r}_i; \mathbf{r}_j; \mathbf{r}_i^0; \mathbf{r}_j^0 \rangle = \frac{Q_i Q_j}{(2\pi\hbar^2)^3} \exp\left[-\frac{d_{ij}(1=2)}{2\hbar^2} U(\mathbf{r}_i; \mathbf{r}_j)\right]; \quad (5)$$

where $d_{ij}(1=2) = \frac{1}{2} \mathbf{r}_{ij} + \mathbf{r}_{ij}^0$. Alternatively, the integral can be simplified by taking the off-diagonal Kelbg potential only at the center coordinate,

$$\langle \mathbf{r}_i; \mathbf{r}_j; \mathbf{r}_i^0; \mathbf{r}_j^0 \rangle = \frac{Q_i Q_j}{(2\pi\hbar^2)^3} \exp\left[-\frac{\mathbf{r}_{ij}^2 + \mathbf{r}_{ij}^0{}^2}{2\hbar^2} U(\mathbf{r}_i; \mathbf{r}_j)\right]; \quad (6)$$

Many authors use the *end-point* approximation (4) for the effective potential $\langle \mathbf{r}_i; \mathbf{r}_j; \mathbf{r}_i^0; \mathbf{r}_j^0 \rangle$ in the pair density matrix (2) due to the fact that it is very convenient computationally. The pair potential for interparticle interaction simply is replaced by an effective potential which has only a dependence on the radial variables $\mathbf{r}_{ij}^2 + \mathbf{r}_{ij}^0{}^2$. However, most of the accuracy is usually lost in this end-point approximation.

Since the Kelbg potential is obtained by first order perturbation theory its application is limited to weak coupling, $\beta \ll 1$, where β is the ratio of mean potential to kinetic energy. In unbound and bound states of an electron-proton pair this results in the following conditions on temperature

$$\begin{aligned} &= \frac{e^2}{r} = k_B T \ll 1 \quad k_B T \ll \frac{e^2}{r} \\ &= Ry = k_B T \ll 1 \quad k_B T \ll Ry; \end{aligned} \quad (7)$$

where $Ry = Ha^2 = e^2/2a_B$, and a_B is the Bohr radius. For the last case the Kelbg potential (and any of the simplifying approximations) can be only valid for temperatures sufficiently above the atomic binding energy, i.e. for the case of hydrogen, $T \ll Ry = k_B \cdot 158\,000$ K. We address this point in more detail in the section IV, where “exact” binding energies and pair correlation functions for an electron-proton pair are compared with the results obtained with the potentials (3) and (4).

B. Improved diagonal Kelbg potential

The limitation of the Kelbg potential to describe quantum systems only when there are no bound states has lead several researchers [1, 30, 31] to introduce and investigate a more generalized form of the quantum potential with an additional free parameter α_{ij}

$$\begin{aligned} V_{ij}(r_{ij}) &= \frac{q_i q_j}{r_{ij}} \left[1 - e^{-\frac{r_{ij}^2}{\alpha_{ij}}} + \frac{r_{ij}}{\alpha_{ij}} \left(1 - \text{erf} \left(\frac{r_{ij}}{\alpha_{ij}} \right) \right) \right]; \end{aligned} \quad (8)$$

This potential has an advantage of preserving the correct first derivative at $r = 0$ of the original Kelbg potential, $(0;)_r^0 = -\frac{q_i q_j}{\alpha_{ij}}$, but at the same time allows to correct the wrong value of the height of the Kelbg potential at $r = 0$, i.e. $(0;) = \frac{q_i q_j}{\alpha_{ij}}$ to include bound states. Using the definition of the effective potential as

$$V_{ij}(r_{ij}) = S_{ij}(r_{ij}); \quad (9)$$

where $S_{ij} = S(r_{ij};)$ is the exact binary Slater sum of particles i, j . The fit parameter α_{ij} in Eq. (8), is related to the Slater sum at zero interparticle distance according to

$$\alpha_{ij} = \frac{q_i q_j}{\ln [S_{ij}(r_{ij} = 0;)]}; \quad (10)$$

It is important to note that α_{ij} depends both on temperature and the type of particles. For example, the binary Slater sum of two electrons at zero separation has the form (including the average “ h ” over possible values of the total spin $S = 0, 1$)

$$\begin{aligned} S_{ee}^{hi}(r_{ee} = 0;) &= 2^{p-} J_1(r_{ee}); \\ J_1(r_{ij}) &= \int_0^\infty e^{-x^2} \frac{x dx}{1 - \exp(-\frac{r_{ij}}{x})}; \end{aligned} \quad (11)$$

where the interaction parameter $\alpha_{ij} = q_i q_j = \alpha_{ij}$.

On the other hand, for an electron-proton pair the Slater sum can be written as

$$\begin{aligned} S_{ep}(r_{ep} = 0;) &= 4^{p-} J_1(r_{ep}) + 3^{p-} Z_3(r_{ep}); \\ Z_n(r) &= \sum_{y=1}^\infty y^n e^{-2y^2 r^2}; \end{aligned} \quad (12)$$

where the last term shows the contribution of the bound states.

The original Kelbg potential was derived for very high temperatures without taking into account exchange between particles. This work was followed by several studies where the pseudopotentials for identical particles have been calculated numerically [32, 33] or analytically [34, 35, 36] using expansions in a quantum parameter, small particle separation, and temperature. In the present work, following these studies, we approach the problem of the pseudopotential with exchange by using the formalism of two-particle density matrices (DM). The pair DM can be calculated numerically (see Sec. II C) or expressed in analytical form (2) using the improved Kelbg potential (8).

In the case of a pair of electrons, they can be in a singlet or triplet state, and the spatial wave function is symmetric or antisymmetric under the exchange of particle indices. Thus, one can define a binary effective electron-electron interaction for three different cases

$$\begin{aligned} U_{ij}^{S(T)} &= \frac{\rho_2(r_i; r_j; r_i; r_j)}{\rho_1(r_i; r_i) \rho_1(r_j; r_j)}; \\ U_{ij}^{hi} &= \frac{3}{4} U_{ij}^{S(T)} + \frac{1}{4} U_{ij}^{S}; \end{aligned} \quad (13)$$

where ρ_1 and ρ_2 are the one- and two-particle density matrices, and U_{ij}^S , U_{ij}^T and U_{ij}^{hi} are the effective interactions in the singlet (S), triplet (T) state and the spin-averaged potential, respectively.

If we now approximate the two-particle DM, ρ_2 , by Eq. (2) and factorize it into the DM’s of the center-of-mass and relative coordinates (the corresponding expressions are given in Sec. II C, cf. Eq. (27)), then we obtain for the pseudopotential between two electrons being in the singlet (triplet) state and for the spin-averaged potential, respectively,

$$U_{ee}^{S(T)} = \frac{1}{2} \ln \left[e^{-U_{ee}(r; r)} e^{-r^2} e^{-\frac{r^2}{2}} e^{-U_{ee}(r; r)} \right] \quad (14)$$

$$U_{ee}^{hi} = \frac{1}{2} \ln \left[e^{-U_{ee}(r; r)} \frac{1}{2} e^{-r^2} e^{-\frac{r^2}{2}} e^{-U_{ee}(r; r)} \right] \quad (15)$$

In this expression, the function, $U_{ee}(r; r)$, is a pseudopotential between distinguishable particles (i.e. calculated without exchange effects). Thus, for it one can substitute the original Kelbg potential, Eq. (4), the improved Kelbg potential, Eq. (8), or any further improved approximation for the binary interaction. In the case of two electrons, if for $U_{ee}(r; r)$ we use the improved Kelbg

potential (8), then the fit parameter γ_{ee} must be obtained from Eq. (10) where for the binary Slater sum one should take the one for two distinguishable particles with Coulomb repulsion

$$S_{ee}^{n \circ \text{exc}}(r_{ee} = 0;) = 4^{\frac{P}{2}} \gamma_{ee} J_1(\gamma_{ee}): \quad (16)$$

As it follows from Eq. (15) an exchange contribution (effect of particle statistics in the pair interaction) arises from the kinetic energy part of the density matrix and the non-diagonal potential, $U_{ee}(\mathbf{r}; \mathbf{r})$, which in the first order of the perturbation theory can be calculated using Eq. (3). A further simplification (which is crucial for application of the pseudopotentials in semiclassical MD simulations presented in Sec. V) can be achieved by approximating the off-diagonal potential by the diagonal terms, $U_{ee}(\mathbf{r}; \mathbf{r}) \approx \frac{1}{2} [U_{ee}(\mathbf{r}; \mathbf{r}) + U_{ee}(\mathbf{r}; \mathbf{r})] = U_{ee}(\mathbf{r}; \mathbf{r})$, and the above expressions are reduced to

$$U_{ee;0}^S(T) = U_{ee}(\mathbf{r}; \mathbf{r}) - \frac{1}{2} \ln \left(1 - e^{-\frac{r^2}{2}} \right) \gamma_{ee}^0; \quad (17)$$

$$U_{ee;0}^{\text{hi}} = U_{ee}(\mathbf{r}; \mathbf{r}) - \frac{1}{2} \ln \left(1 - \frac{1}{2} e^{-\frac{r^2}{2}} \right) \gamma_{ee}^0: \quad (18)$$

We can note that in the diagonal approximation for the potential, the exchange term corresponds to the case of the ideal Fermi gas (i.e. exchange without interaction), the exchange term arising from the interaction is missing.

Taking in Eq. (17) the limit $r \rightarrow 0$ we see that the potential of the triplet state shows a logarithmic divergency

$$U_{ee;0}^T = U_{ee}(\mathbf{r}; \mathbf{r}) - 2k_B T \ln \left(\frac{r}{\gamma_{ee}} \right) + O \left(\frac{r^2}{\gamma_{ee}^2} \right); \quad (19)$$

whereas the singlet and the spin-averaged potential acquires an additional exchange contribution

$$U_{ee;0}^{S, \text{hi}} = U_{ee}(\mathbf{r}; \mathbf{r}) - k_B T \ln f_2 g + O \left(\frac{r^2}{\gamma_{ee}^2} \right); \quad (20)$$

but the slope of these potentials at the origin are same as in the case without exchange. This means, in case of Coulomb interaction, the slope is defined by the slope of the original Kelbg potential γ_{ee}^0 ,

$$U_{ee}(\mathbf{r}; \mathbf{r}) \Big|_{r=0} = \gamma_{ee}^0(0) \left(\frac{e^2 r}{2} + O \left(\frac{r^2}{\gamma_{ee}^2} \right) \right); \quad (21)$$

In our previous paper [1] we reported on the temperature dependence of the fitting parameter γ_{ij} for the electron-electron and electron-proton interactions. There, two types of calculations have been presented. First, the values of $\gamma_{ij}(T)$ were obtained by a least-square fit of the improved diagonal Kelbg potential (IDKP), the Eq. (8), to the “exact” pair potential U (see Eq. (27)), and second, from Eq. (10) by evaluating the values of the binary Slater sums. It has been found that both methods agree within the statistical uncertainty.

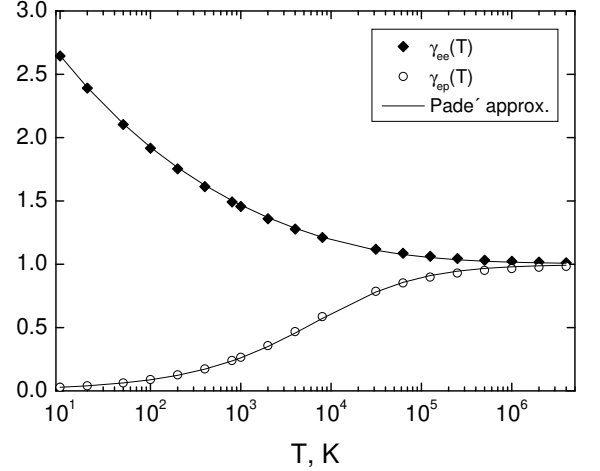


Figure 1: Temperature dependence of the fit parameter for the binary interactions: electron-proton, $\gamma_{ep}(T)$, and electron-electron (no exchange), $\gamma_{ee}(T)$. Symbols show the γ -values obtained with the least-square fit of the IDKP to the “exact” pair potential without exchange. Solid curves correspond to the Padé approximation (22,23).

Extending our earlier results, we now present a Padé approximation which contains an analytical temperature dependence of the parameters γ_{ij} which will be useful for practical applications,

$$\gamma_{ep}(T) = \frac{x_1 + x_1^2}{1 + a_{ep} x_1 + x_1^2}; \quad (22)$$

$$\gamma_{ee}(T) = \frac{\gamma_{ee}(T \rightarrow 0) + a_{ee} x_1 + x_1^2}{1 + x_1^2}; \quad (23)$$

where $x_1 = \frac{P}{8 k_B T} \frac{H a}{H a} = \frac{P}{8 k_B T} \frac{H a}{H a}$ (with the Hartree energy, $H a = 2 R y = 315\,775$ K), $a_{ep} = 1.090(14)$, $a_{ee} = 0.18(1)$. The limit value, $\gamma_{ee}(T \rightarrow 0)$, has been obtained from Eq. (10) by evaluating the zero temperature limit of the binary Slater sum (16)

$$\gamma_{ee}(T \rightarrow 0) = \frac{2}{P} x^3 \frac{1}{\ln f_8 x^4 - \frac{P}{g} - 3x^2}; \quad (24)$$

with $x = (\frac{1}{2} \gamma_{ee} - 2)^{\frac{1}{3}}$. The excellent accuracy of the Padé approximation is demonstrated in Fig. 1.

In Fig. (1) we present the temperature dependence of γ_{ij} obtained from the least-square fit (full and open symbols) to the “exact” pair potential of distinguishable particles (no exchange) and Padé approximation (22) (solid curves). The most important result is that the corrected Kelbg potential is now *not limited to weak coupling* as is the original Kelbg potential. For the case $\gamma_{ij} = 1$, Eq. (8) coincides with Eq. (4). One clearly sees the deviation of γ_{ij} from unity for $T > 10^6$ K, which shows that the quantum extension of particles is becoming influenced by interaction effects and is now of the order of

$\tilde{\psi}_{ij} = \psi_{ij}$, instead of the original thermal DeBroglie wavelength λ_{ij} . Thus, with the Padé formulas (22-23), we have obtained an analytical fit for the quantum extension of the scattering particles.

The Padé approximations (22), (23) have been successfully used in quasi-classical molecular dynamics simulations of two-component hydrogen plasmas. As we show in Sec. V, they allow to obtain accurate results for partially hydrogen (or other quantum systems of oppositely charged particles with bound states).

Finally, we want to note that, in the MD simulations of quantum plasmas, it can be advantageous to have spin-dependent potentials for the electron subsystem defined by Eqs. (14) or (17). The spin-resolved approximation allows for a refined modelling, for example, it allows for the description of molecule formation, spin density waves, spin flip processes in the presence of a magnetic field and so on.

C. Effective potentials from numerical solution of two-body Bloch equation

In the present section, we briefly describe the numerical methods which have been used to solve the two-particle problem in order to obtain the “exact” quantum pair potentials. These results have been used to obtain the analytical fit in the improved Kelbg potential. Furthermore, they will be used to test the accuracy of various analytical approximations for the quantum pair potentials in Sec. III below.

Let us factorize full two-particle density matrix into a center-of-mass term and a density matrix of relative coordinates

$$\langle \mathbf{r}_i; \mathbf{r}_j; \mathbf{r}_i^0; \mathbf{r}_j^0 \rangle = \langle \mathbf{R}; \mathbf{R}^0 \rangle \langle \mathbf{r}; \mathbf{r}^0 \rangle; \quad (25)$$

where $\mathbf{R} = (m_i \mathbf{r}_i + m_j \mathbf{r}_j) / (m_i + m_j)$, and $\mathbf{r} = \mathbf{r}_i - \mathbf{r}_j$, and analogously for $\mathbf{R}^0; \mathbf{r}^0$. When for the relative DM in the analogy with the Eq. (2) we can define the effective pair potential as

$$\langle \mathbf{r}; \mathbf{r}^0 \rangle = \langle \mathbf{r}_{\text{kin}} \rangle \langle \mathbf{r}; \mathbf{r}^0 \rangle e^{-U(\mathbf{r}; \mathbf{r}^0)}; \quad (26)$$

which results in the following expression

$$U(\mathbf{r}; \mathbf{r}^0) = -\ln [\langle \mathbf{r}; \mathbf{r}^0 \rangle / \langle \mathbf{r}_{\text{kin}} \rangle]; \quad (27)$$

where $\langle \mathbf{r}; \mathbf{r}^0 \rangle_{\text{kin}}$ is the kinetic energy DM.

One of the possibilities to get the relative density matrix $\langle \mathbf{r}; \mathbf{r}^0 \rangle$ is to directly solve the corresponding one-particle Schrödinger equation and calculate the DM as a contribution from bound and continuum states. This procedure is advantageous when the Schrödinger equation can be solved analytically and we know analytical expressions for contributions of scattering and bound states, as for example for Coulomb potential, e.g. [36]. But if it is not the case, a separate calculation of each

matrix element for each new values of end-points \mathbf{r} and \mathbf{r}^0 will be not efficient and time-demanding procedure. In principle, such calculations can be done in advance with $U(\mathbf{r}; \mathbf{r}^0)$ be stored in the tables of the potential, but one still needs to solve the Schrödinger equation many times for each value of quantum numbers and also for wavefunctions of continuum states.

It is possible to approach to this problem from the other side and calculate the DM directly without solving the Schrödinger equation. In this work we apply two efficient methods – the *matrix squaring technique* [32, 37] and the Feynman-Kleinert *variational approach* [38, 39]. In the Sec. III we will compare an accuracy of the pseudopotentials obtained with these methods.

1. Matrix squaring technique

The exact off-diagonal pair density matrix can be calculated efficiently by this method introduced by Storer and Klemm [32]. For the case of spherical symmetry of the interaction potential, the relative pair density matrix in the Eq. (25) is expanded in terms of partial waves. This expansion reads, for the two- and three-dimensional cases,

$$\langle \mathbf{r}; \mathbf{r}^0 \rangle = \frac{1}{2} \sum_{l=0}^{\infty} \frac{x^l}{r r^0} \langle \mathbf{r}; \mathbf{r}^0 \rangle_l e^{i l \theta}; \quad (28)$$

$$\langle \mathbf{r}; \mathbf{r}^0 \rangle = \frac{1}{4} \sum_{l=0}^{\infty} \frac{x^l}{r r^0} (2l+1) \langle \mathbf{r}; \mathbf{r}^0 \rangle_l P_l(\cos \theta);$$

where θ is the angle between \mathbf{r} and \mathbf{r}^0 . Each partial-wave component satisfies the 1D Bloch equation for a single particle in an external potential given by the interaction potential and also a convolution equation,

$$\langle \mathbf{r}; \mathbf{r}^0 \rangle = \int_0^{\infty} d\mathbf{r}^{\text{co}} \langle \mathbf{r}; \mathbf{r}^{\text{co}} \rangle \langle \mathbf{r}^{\text{co}}; \mathbf{r}^0 \rangle; \quad (29)$$

This is the basic equation of the *matrix-squaring method* which allows to calculate the function $\langle \mathbf{r}; \mathbf{r}^0 \rangle$ at a given temperature T from the same function at a two times higher temperature. Squaring the density matrix k times results in a lowering of the temperature by a factor of 2^k . Each squaring involves only a one-dimensional integration which, due to the Gaussian-like nature of the integrand in Eq. (29), can be performed quite accurately and efficiently by standard numerical procedures. To start the matrix-squaring iterations, Eq. (29), one needs a known accurate high-temperature form for the density matrix. A convenient choice is the semiclassical approximation

$$\langle \mathbf{r}; \mathbf{r}^0 \rangle = \langle \mathbf{r}; \mathbf{r}^0 \rangle_0 \exp \left[-\frac{1}{\hbar} \int_{\mathbf{r}^0}^{\mathbf{r}} \sqrt{V(\mathbf{x})} d\mathbf{x} \right]; \quad (30)$$

where $\rho_1^0(\mathbf{r}; \mathbf{r}^0)$ is the partial-wave component of the free-particle density matrix.

Once the pair density matrix $\rho_1(\mathbf{r}; \mathbf{r}^0)$ is computed for the desired value of β , it is substituted into Eqs. (28-29), and a summation over partial waves readily yields the full relative density matrix.

2. Variational perturbation approach

As a second method for solving the off-diagonal Bloch equation we used a *variational perturbation expansion* developed by Feynman and Kleinert [38]. In this procedure the initial density matrix is presented in the form of a trial path integral which consists of a suitable superposition of local harmonic oscillator path integrals centered at arbitrary average positions \mathbf{x}_m , each with its own frequency squared $\omega_m^2(\mathbf{x}_m)$. One starts from decomposing the action in the density matrix as

$$\rho(\mathbf{r}; \mathbf{r}^0) = \int \mathcal{D}\mathbf{x} e^{A[\mathbf{x}]} \rho_1(\mathbf{r}; \mathbf{r}^0); \quad (31)$$

$$A[\mathbf{x}] = A_{\mathbf{x}_m}[\mathbf{x}] + A_{\text{int}}[\mathbf{x}]; \quad (32)$$

with $A_{\mathbf{x}_m}[\mathbf{x}]$ being the action of a trial harmonic oscillator with the potential minimum located at \mathbf{x}_m , and \mathcal{D} being the functional integral over all trajectories. The interaction part

$$A_{\text{int}}[\mathbf{x}] = \int_0^\beta d\tau V[\mathbf{x}(\tau)] - \frac{1}{2} \omega_m^2[\mathbf{x}(\tau) - \mathbf{x}_m]^2; \quad (33)$$

is defined as the difference between the original potential $V(\mathbf{x})$ and the displaced harmonic oscillator. The ω_m^2 term in Eq. (33) compensates the contribution of $A_{\mathbf{x}_m}[\mathbf{x}]$ in Eq. (32). Now one can calculate the density matrix (31) by treating the interaction (33) as a perturbation, leading to a moment expansion

$$\begin{aligned} \rho(\mathbf{r}; \mathbf{r}^0) &= \int_0^{\beta} d\tau \rho_1(\mathbf{r}; \mathbf{r}^0) + \frac{1}{\beta} \int_0^{\beta} d\tau \int_0^{\beta} d\tau' A_{\text{int}}[\mathbf{x}(\tau)] \rho_1(\mathbf{r}; \mathbf{r}^0) + \dots \\ &= e^{-W_N} \frac{1}{2^{\frac{N-1}{2}}} \int_0^{\beta} d\tau \rho_1(\mathbf{r}; \mathbf{r}^0); \end{aligned} \quad (34)$$

with the definition

$$\begin{aligned} W_N &= \frac{d}{2} \ln \frac{\sinh \beta \omega_m}{\beta \omega_m} + \frac{1}{2\beta} \frac{\cosh \beta \omega_m - 1}{\omega_m^2} \\ &= \frac{1}{2\beta} \sum_{n=1}^N \frac{(-1)^{n-1}}{n^{N-n}} \int_0^{\beta} d\tau \int_0^{\beta} d\tau' A_{\text{int}}[\mathbf{x}(\tau)] \rho_1(\mathbf{r}; \mathbf{r}^0); \end{aligned} \quad (35)$$

where d is the space dimensionality and N the order of the approximation. The function $\rho_1^0(\mathbf{r}; \mathbf{r}^0)$ is the trial

harmonic oscillator density matrix, $\rho_1 = \rho_1(\mathbf{r}; \mathbf{r}^0)$; $\rho_1^0 = \rho_1^0(\mathbf{r}; \mathbf{r}^0)$, and the expectation value of the interaction action on the r.h.s. of Eq. (35) is given by

$$\begin{aligned} \langle A_{\text{int}} \rangle &= \frac{1}{\int \mathcal{D}\mathbf{x} e^{A[\mathbf{x}]} \rho_1(\mathbf{r}; \mathbf{r}^0)} \int \mathcal{D}\mathbf{x} A[\mathbf{x}] e^{A[\mathbf{x}]} \rho_1(\mathbf{r}; \mathbf{r}^0) \\ &= \int \mathcal{D}\mathbf{x} A[\mathbf{x}] \rho_1(\mathbf{r}; \mathbf{r}^0) / \int \mathcal{D}\mathbf{x} \rho_1(\mathbf{r}; \mathbf{r}^0); \end{aligned} \quad (36)$$

The function W_N can be identified as an *effective quantum potential* which is to be optimized with respect to the variational parameters $\omega_m^2(\mathbf{r}; \mathbf{r}^0)$; $\mathbf{x}_m(\mathbf{r}; \mathbf{r}^0)$. Note that, in the high temperature limit, this effective potential goes over to the original potential $V(\mathbf{r})$. The optimal parameter values are determined from the extremity conditions

$$\frac{\partial W_N}{\partial \omega_m^2} = 0; \quad \frac{\partial W_N}{\partial \mathbf{x}_m} = 0; \quad (37)$$

The perturbation series (35) is rapidly converging, in most cases already in the first-order approximation W_1 for the effective potential, and gives a reasonable estimate of the desired quantities.

III. COMPARISON OF THE PAIR POTENTIALS AND THEIR TEMPERATURE DEPENDENCE

We will now compare accuracy of the pair potentials discussed above (or two-particle density matrices corresponding to these potentials), their temperature dependence and range of applicability.

A. Full density matrix of electron-proton pair

In Fig. 2 we show the angular dependence of the full off-diagonal two-particle density matrix calculated with the off-diagonal Kelbg potential – ODKP (3) and its diagonal approximation – DKP (4). The density matrix is shown at several temperature values ($T = 1\,000\,000$; $250\,000$ and $62\,500$ K) and several angular distances ($\theta = 0$; $\theta = 2$) between the vectors $\mathbf{r} = \mathbf{r}_{ij}$; $\mathbf{r}^0 = \mathbf{r}_{ij}^0$ (in each of the figures, the top curves correspond to the case of parallel vectors, $\theta = 0$, the lowest curves to antiparallel vectors, $\theta = \pi$). Also, for reference, we give the off-diagonal density matrix obtained from the ‘exact’ solution of the Bloch equation, cf. Sec. II C 1. At high temperatures, $T = 250\,000$ K, the Kelbg density matrix does not exhibit large deviations from the exact result. At $T = 1\,000\,000$ K, the ODKP density matrix practically coincides with the exact solution, whereas the DKP approximation shows small deviations. In these cases the perturbation expansion applies, $\beta \omega_m^2 \ll 1$, see left column of Fig. 2. With decreasing temperature, the deviations

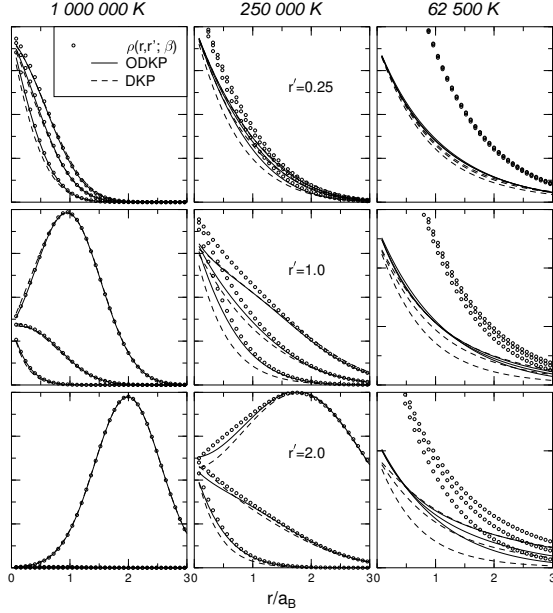


Figure 2: The “exact” off-diagonal density matrix $\rho(r, r'; \beta)$ for an electron-proton pair vs. the density matrix calculated with the diagonal (DKP) and off-diagonal (ODKP) Kelbg potentials. In all figures, results for three angular values are given $\beta = 0$ (upper curves), $\beta = 2$ (middle) and $\beta = 0$ (lower curves). The proton is located at the origin, and the vector \mathbf{r}^0 (initial electron position) is fixed, $\mathbf{r}^0 = 0.25; 1.0; 2.0$. The vector \mathbf{r} (final electron position) is varied, β is the angle between the vectors \mathbf{r} and \mathbf{r}^0 .

from the exact results grow, see middle column. To better understand the details of the deviations, we magnified them by including also results for $T = 62\,500\text{ K}$, which is far beyond the scope of the perturbation theory, $T = 0.4\text{ Ry} = k_B$, i.e. $\beta = 2.5$. Here we observe that, at the origin, the density matrix of the Kelbg potential is 3 times less than the exact one. The largest errors were found for the DKP, in particular, in the case when the vectors $\mathbf{r}; \mathbf{r}^0$ have the opposite direction ($\beta = \pi$).

The behavior of the full density matrix can be understood from the following considerations. The density matrix results from contributions of kinetic and potential energy operators, cf. Eq. (1). At small distances ($r^0 = 0.25$) the Coulomb attraction between an electron and a proton dominates and, therefore, the density matrix shows an exponential decay. At the largest distance ($r^0 = 2.0$) kinetic and potential energy are of the same order and a Gaussian-like free particle density matrix emerges, as can be clearly seen in the bottom left part of Fig. 2.

From this first comparison we can conclude that both, the DKP and the ODKP, show satisfactory agreement with the exact result in the cases where perturbation theory applies, $T \gtrsim 2\text{ Ry}$. At lower temperatures there is only qualitative agreement. The strongest deviations arise for small interparticle distances \mathbf{r}, \mathbf{r}^0 , and this, as

will be shown below, results from the incorrect height of the Kelbg potential at zero distance $r = 0$.

B. Effective interaction of electron-proton and electron-electron pairs

In Fig. 3(a,b) we show and compare the accuracy of several effective electron-proton potentials and their temperature derivatives obtained by various methods. As an “exact” reference potential to which the accuracy of other potentials is compared we use U_{pair} obtained from the electron-proton pair density matrix calculated with the matrix squaring technique.

First, we note from Fig. 3(a) that, at given temperatures $T \gtrsim 2\text{ Ry}$, the original Kelbg potential shows the largest deviations from the “exact” result, U_{pair} . While the spatial derivative of the DKP coincides with that of U_{pair} , a systematic offset of the DKP compared to U_{pair} is observed at the origin $r = 0$, which increases when the temperature is lowered. The agreement is satisfactory only for the curve corresponding to $T = 320\,000\text{ K}$. The accuracy of the Kelbg potential becomes worse for quantities involving its temperature derivative. For example, for the total energy one has to compute the thermodynamic average of the function $\mathcal{Q}(U) = \mathcal{Q}(U_{\text{Kelbg}})$. This function is shown in Fig. 3(b). If multiplied by the Boltzmann factor e^{-U} , this function is a good estimate for the binding energy (E_b) of an electron-proton pair. In the case of a bound state the main contribution to the energy comes from the region of small interparticle distance, $r \lesssim 3a_B$. Therefore, the behavior of $\mathcal{Q}(U) = \mathcal{Q}(U_{\text{Kelbg}})$ near the origin determines the accuracy of the calculations of the energy and other thermodynamic quantities. As we can see from the curve for 5000 K in Fig. 3(b), the depth of the DKP is much less than that of U_{pair} and, therefore, it gives a too low binding energy of $E_b = 0.16\text{ Ha}$, i.e. a factor of three too low compared with the true ground state energy $E_b^0 = 0.5\text{ Ha}$.

As it was already discussed in Sec. IIB the accuracy of the DKP can be improved with the additional fit parameter α_{ij} . In Fig. 3(a,b) this potential is denoted as K_{elbg} . One can see that at all considered temperatures K_{elbg} practically coincides with U_{pair} . Even in the case of the strong coupling ($T = 5000\text{ K}$) the agreement is very good.

The next potential shown in this figure is the variational potential, $W^{(1)}_{\text{var}}$, introduced in the Sec. IIC2. This potential is more accurate than the DKP and qualitatively reproduces the “exact” effective pair potential U_{pair} for temperatures $T = 125\,000\text{ K}$, $320\,000\text{ K}$ and its derivative (see Fig. 3(b)). The key point is that the *variational perturbation theory* [38] replaces the perturbation expansion in β (which does not converge for $\beta \gtrsim 1$) into another expansion, Eq. (34), which does not have this restriction. The results of this approach can be improved by taking into account higher order terms in Eq. (34) (the results shown in the figure include only the first term,

$n = 1$). The convergence of Eq. (34) extends even to very strong coupling and has been successfully applied in field theory [39].

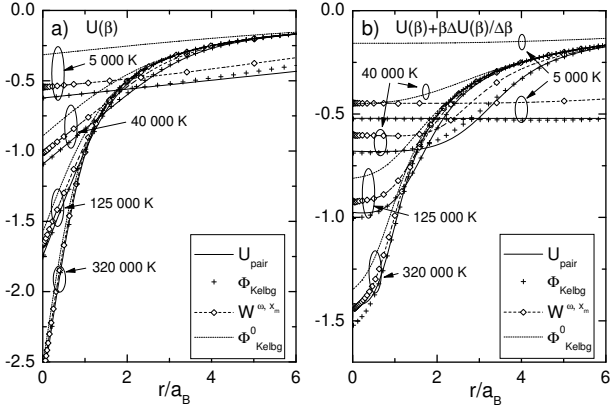


Figure 3: (a): Diagonal effective electron-proton potential (in units of Ha) for several cases: the DKP $U^0(\mathbf{r}; \beta)$ (4), the improved DKP $U^1(\mathbf{r}; \beta)$ (8), variational potential $W_1^{ex}(\mathbf{r}; \beta)$ (35), pair potential U_p (27) corresponding to the “exact” density matrix. Each potential is given at three temperature values: 5 000; 40 000; 125 000 and 320 000 K. (b): the function $U(\beta) + \beta \Delta U(\beta) / \Delta \beta$ for the same approximations and temperatures.

We mention that comparison with other effective potentials has been performed in our paper [1]. In particular, the “exact” pair potential was compared with the results of Barker [33] (the calculations of the pair potential by the direct eigenfunction summation) and the Deutsch potential. A good agreement has been found with the data of [33], while the deviations of the Deutsch potential turned out to be slightly larger than that of the Kelbg potential. The reason is that the Deutsch potential has an incorrect spatial derivative, U_r^0 , for $r > 3a_B$.

Next, in Fig. 4, we compare pair distribution functions (PDF) of two electrons in a singlet and triplet states for different temperatures, obtained from the expression with the effective potential

$$g(\mathbf{r}) / e^{-U^S(\mathbf{r}; \beta)} : \quad (38)$$

Due to the Pauli principle in Fig. 4(a) the PDF is goes to zero as $r_{ee} \rightarrow 0$. On the other hand, for electrons in a singlet state (Fig. b) this happens only if the temperature is decreased down to 31 250 K, when the potential energy dominates over the kinetic energy. The three lines in Fig. 4(a) show the cases when as an effective potential in the Eqs. (15-17) we substitute the “exact” pair potential and the Kelbg potential. In the last case, Eq. (17), the exchange contribution from the potential function is neglected. This, as shows Fig. 4(a), becomes important only for the temperature 31 250 K and below. But the overall accuracy of the Kelbg potential for a description of two particles with the same charge (even without improving its value at the origin with U^0) is significantly

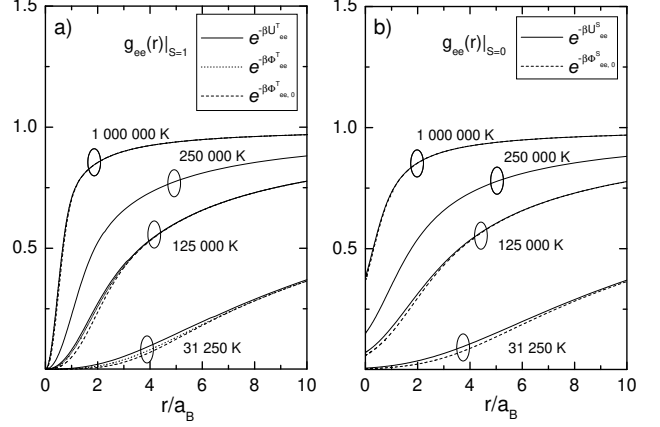


Figure 4: Pair distribution function for a pair of electrons. a: In a triplet state (parallel spins, $S = 1$); b: In a singlet state (antiparallel spins, $S = 0$). Cases compared are: Eq. (14), using for U_{ee} the “exact” pair potential and the Kelbg potential, U_{ee}^0 , respectively, as well as the simpler expression, Eq. (17) with the Kelbg potential. The pair distribution functions are shown for four temperatures, $T = 31\,250$, 125 000, 250 000 and 1 000 000 K.

better (compared to the results with the “exact” pair potential) than for particles with opposite charge, cf. Fig. 3. This is due to absence, in this case, of contributions from bound states.

The pair correlation functions at $T = 125\,000$ K can be compared with those for a hydrogen plasma obtained by molecular dynamics simulations, see Fig. 9. One can see that, at least at this temperature, the electron-electron PDF’s of that many-particle simulation look quite similar to the two-particle case shown in Fig. 4. Some differences are noticeable for the value of g_{ee} at $r = 0$ as the density is increased from $r_s = 6$ to $r_s = 4$, see Sec. V.

In the next section we discuss application of quantum pair potentials in thermodynamical calculations using Feynman trajectories in imaginary time (PIMC).

IV. QUANTUM PAIR POTENTIALS IN PATH INTEGRAL MONTE CARLO

It is well known (see for example discussion in Chapter 12 of [38]) that the singularity of the attractive Coulomb potential causes difficulties in the euclidian path integral. If based on Feynman’s original path integral representation, a path consists of a *finite* number of straight pieces, each with a classical euclidian action, containing the singular Coulomb potential. However, in this case, the energy of the path can be lowered indefinitely by an almost stretched configuration which corresponds to a slowly moving particle sliding down to the $e^2 = r$ abyss. This phenomenon is called *path collapse*.

One possibility to prevent this effect is to use a modified “regularized” Coulomb potential which has a cutoff

at $r = 0$. This procedure, however, is quite arbitrary, and the results are sensitive to the used cutoff parameters. Of course, in nature, these difficulties are prevented by quantum fluctuations which equip the path with a configurational entropy. The latter must be sufficiently singular to produce a regular free energy bounded from below. The inclusion of quantum fluctuations in the Euclidean action of the Feynman path pieces smoothes the singular Coulomb potential, producing an effective potential that is finite at the origin, and the *path collapse* is avoided. This again shows the importance of effective potentials, specifically, in “quasiclassical” simulations (classical Monte Carlo and molecular dynamics methods). Of great importance are potentials which have a closed analytical form. In this case for many thermodynamical quantities it is possible to obtain analytical solutions.

For simulations of correlated quantum many-body systems which are based on *first principles*, the initial many-body hamiltonian with the true singular Coulomb energy operator is to be considered and solved to find some effective many-body interaction potential. For this it is important that in the high-temperature limit the N -particle density matrix can be expanded in terms of 2-particle, 3-particle etc. contributions. If the temperature is sufficiently high then all contributions except the first one, taking into account two-particle correlations, can be omitted. As a result, the following approximation for the N -particle density matrix holds

$$\langle \mathbf{R}; \mathbf{R}^0; \rangle = \sum_{i,j < k} \frac{\rho^{[2]}(\mathbf{r}_j; \mathbf{r}_k; \mathbf{r}_i^0; \mathbf{r}_k^0;)}{\rho^{[1]}(\mathbf{r}_i; \mathbf{r}_i^0;)} \rho^{[1]}(\mathbf{r}_k; \mathbf{r}_k^0;)} + O(\rho^{[3]}); \quad (39)$$

where $\mathbf{R} = \{\mathbf{r}_1; \dots; \mathbf{r}_N\}$ specifies coordinates of all N particles, $\rho^{[1]}$ ($\rho^{[2]}$) is the single (two) particle density matrix. The above *pair* approximation is usually used in PIMC simulations [37]. The N -particle density matrix $\langle \rangle$ contains a complete information about the system with the observables given by

$$\langle \hat{O} \rangle = \frac{\text{Tr}[\hat{O} \hat{\rho}]}{\text{Tr}[\hat{\rho}]} = \frac{\int d\mathbf{R} \langle \mathbf{R} | \hat{O} | \mathbf{R} \rangle \rho(\mathbf{R})}{\int d\mathbf{R} \rho(\mathbf{R})}; \quad (40)$$

Due to the exponential form, the N -particle density operator $\hat{\rho} = e^{-\beta \hat{H}}$ can be factorized (in analogy to the matrix squaring method above) as $\hat{\rho} = \hat{\rho}^M$ with $M = \beta/\beta_0$. Consequently, the N -particle density operator $\hat{\rho}$ is expressed in terms of density operators at an M times higher temperature $\beta_0 = \beta/M$. If M is chosen sufficiently large then one can apply the pair approximation (39). Thus, accurate results for the quantum pair potentials and, consequently, the pair density matrix, will allow to compute the density matrix of the whole N -particle system. Here we are not interested in

the investigation of the accuracy of approximation (39) but concentrate on the two-body problem where Eq. (39) is exact.

It is clear that the observables (40) computed with the approximate pair-density matrix $\rho^{[2]}$ contain an error of the order $O(1/M^2)$. Below we will investigate the convergence, as a function of M , of main thermodynamic properties (total energy and e-p pair distribution) for an electron-proton pair using for the pair density matrix $\rho^{[2]}$ results computed with the off-diagonal and the diagonal Kelbg potential.

A. Comparison of diagonal and off-diagonal Kelbg potential on the example of Hydrogen atom

We consider a hydrogen atom in a box with periodic boundary conditions (box size, $L = 20 a_B$) at several temperatures, $T = 31\,250 - 62\,500$ K, when the hydrogen atom can ionize into free particles, as well as for the case $T < 10\,000$ K, when there is essentially only the contribution from the atomic ground state. First, in Fig. 5 we show the e-p pair distribution functions (normalized to the volume $dV = 4\pi r^2 dr$).

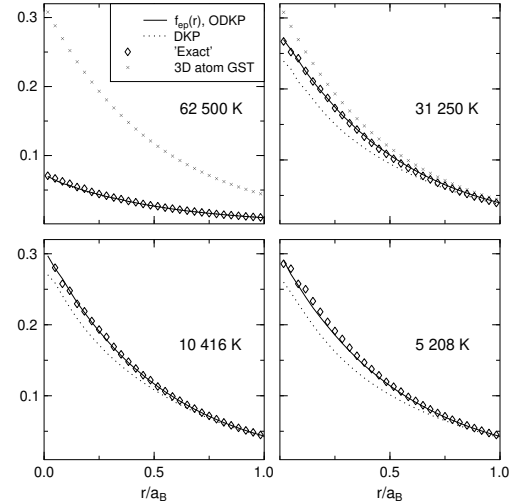


Figure 5: Proton-electron pair correlation functions from PIMC simulations with the “exact” pair density matrix (diamonds), the DKP (dots) and the ODKP (full line). Temperature values are as indicated in the figure parts: $T = 5\,208; 10\,416; 31\,250$ and $62\,500$ K. For comparison, ‘3D GST’ – denotes the pair correlation function corresponding to the ground state of a hydrogen atom.

For temperatures $T = 5\,208$ K and $10\,416$ K the hydrogen atom does not decay into free particles during the duration of a typical simulation run ($\sim 10^6$ Monte Carlo steps). In the figures, the “exact” pair correlation function is compared with the one obtained with the off-diagonal and diagonal Kelbg potentials, respectively (the number of factorization factors for the density matrix was chosen to be $M = 400$). We found that the best accuracy is achieved for the off-diagonal Kelbg potential and

$M = 200$, in this case the ODKP pair correlation function is very close to the exact one.

At elevated temperatures, $T = 31\,250\text{ K}$ and $62\,500\text{ K}$, ionization of the hydrogen atom occurs, but due to the periodic boundary conditions, the free particles cannot go to infinity but, when reaching the boundary, are returned back in the simulation box and have a finite probability for a formation of a bound state again. Thus, this simulation captures the region of partial ionization. As the temperature is increased the ionization probability also increases, leading to a significant drop in the height of the proton-electron pair distribution function at the origin compared to the ground state probability function $\rho_0(r)$, (see Fig. 5, plots for $T=31\,250\text{ K}$ and $T=62\,500\text{ K}$).

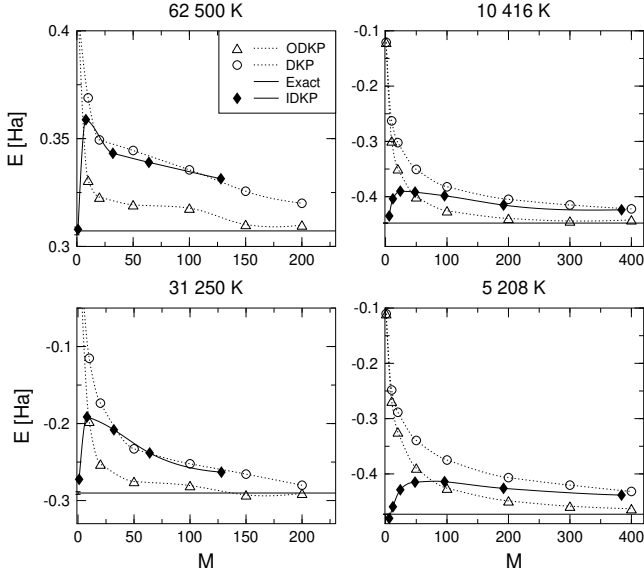


Figure 6: PIMC results for the internal energy of the proton-electron pair using “exact” pair density matrix, DKP, ODKP and Improved Kelbg potential vs. different number of factorization factors M .

In Fig. 6 we analyze the convergence of the internal energy in PIMC simulations with varying number of high-temperature factors M . In particular, we compare independent simulations with the diagonal and off-diagonal Kelbg density matrices, respectively. The “exact” energy value for the considered temperatures is given by the solid line and is obtained from PIMC simulations using the “exact” pair density matrix, cf. Sec. II C 1). The internal energy was obtained using the thermodynamic estimator, $E = -\frac{1}{\beta} \ln Z$, where Z is the partition function. Comparing the *diagonal* and *off-diagonal* cases one can note that the ODKP density matrix shows much better and faster convergence to the exact energy value. A simple estimate shows that the relative error of the total energy, in the diagonal approximation, depends on factorization number M as $E = E_{\text{exact}} + \frac{1}{M}$; $\frac{E - E_{\text{exact}}}{E_{\text{exact}}} = \frac{1}{M}$. In contrast, using the off-diagonal potential, the error converges much faster, $E = E_{\text{exact}} + \frac{1}{M^3}$.

This fact is illustrated in Fig. 7 where the logarithm

of the relative error, $\log(E - E_{\text{exact}})$, is shown as a function of the inverse of the temperature used in the high-temperature factors, $1/T$. In this figure we compare the behavior of the error for the same set of temperatures as in Fig. 6. In Fig. 6 we also add simulation results using *improved diagonal* Kelbg potential (solid line). Its accuracy is better than that of the ODKP at low temperatures (small values of M) but at high temperatures both are comparable.

The main conclusion that can be drawn from the presented PIMC results is that, at equal number of factorization factors M , simulations with the off-diagonal Kelbg potential are significantly more accurate in reproducing the “exact” thermodynamic results of a hydrogen atom. Besides, the full off-diagonal density matrix contains valuable information about the spatial electron distribution around the proton, which is lost in the endpoint approximation. Further, we expect that the best results will be obtained using an *improved off-diagonal* Kelbg potential, which has the correct zero-point value and contains the complete angular dependence of the pair density matrix which, however, is beyond the scope of the present paper.

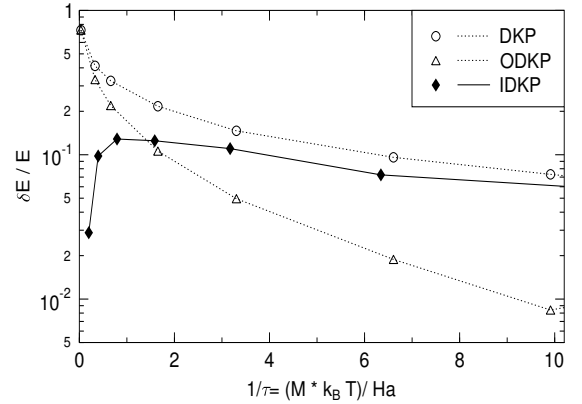


Figure 7: Relative error in the internal energy of the proton-electron pair from PIMC simulations with diagonal, off-diagonal Kelbg potential vs. temperature argument in the two-particle density matrix $1/T$.

V. MOLECULAR DYNAMICS SIMULATIONS

In this section, we apply the improved Kelbg potentials in classical molecular dynamics simulations of dense hydrogen. Classical MD simulations of dense plasmas have been performed by many authors before where the divergency at zero distance leading, in particular, to the classical collapse of an electron into a proton, is usually avoided by some cutoff or “regularization” of the Coulomb potential at small distances. Using in this paper, effective quantum pair potentials obtained from the exact solutions of the Bloch equations, we expect to be on well founded grounds regarding the correct pair interactions

at short distances. This should not only prevent any collapse but also correctly reproduce the formation of hydrogen atoms and thus allow us to obtain essentially improved MD simulation results. On the other hand, this is not a trivial question, since these potentials are derived from pure equilibrium considerations, and there is no ad-hoc proof that they will necessarily be accurate for the description of dynamical behavior as well, in particular under strong non-equilibrium conditions. We, therefore, concentrate in the present analysis on correlated partially ionized hydrogen in *thermodynamic equilibrium*. The results obtained below confirm that, indeed (at least in equilibrium), the quantum pair potentials are well suited for use in the interparticle force terms in classical MD.

Classical MD simulations incorporate all interparticle collision processes and are thus not restricted with respect to the coupling parameter r_s in a classical system. With the use of effective quantum pair potentials, we expect, in addition, to capture dominant features of the quantum nature of microparticles, such as quantum diffraction and spin effects. Thus, these simulations could be called “semiclassical” MD. Having access not only to improved electron-ion potentials but also to spin-dependent electron-electron potentials, allows us to consider also spin effects by simulating electrons with different spin projections as two independent particle species. No spin-flip processes, as they would be expected e.g. in strong magnetic fields are considered [40], but our model should be capable to describe related phenomena as well. In this paper we focus on static properties, such as internal energy, and radial distribution functions. Investigation of dynamical properties and of spin density fluctuation is the aim of a forthcoming paper.

We consider a dense, degenerate hydrogen plasma at two densities corresponding to the Brueckner parameter $r_s = r_{sB} = 4$ and $r_s = 6$ and temperatures $T = 31\,250; 50\,000; 62\,500; 125\,000$ and $166\,670$ K. These parameter values correspond, respectively, to $\beta = 2.53, 1.58, 1.26, 0.63$ and 0.47 , for $r_s = 4$, and $1.68, 1.05, 0.84, 0.42, 0.32$, for $r_s = 6$.

The simulation box of our system, with the length $L = [n_p(N_p + N_e^+ + N_e^-)]^{1/3}$, contains $N_p = 200$ protons, $N_e^+ = 100$ electrons with spin up and an equal number of electrons, $N_e^- = 100$, with spin down. We keep the condition of the electro neutrality by taking $N_p = N_e^+ + N_e^-$. Details of the used numerical algorithm can be found in Ref. [22].

Since MD, in contrast to PIMC, involves only diagonal interaction potentials, we choose the following expressions: for the interaction between electrons and protons, protons and protons and electrons with opposite spin, we use the improved Kelbg potential, Eq. (8), with the fit parameters given by Eqs. (22) and (23), respectively. The interaction between electrons with the same spin projection is described by the diagonal antisymmetric potential, Eq. (17). Further, to properly account for the long range-character of the potentials, we used the standard Ewald procedure as in Ref. [22] whereas, in

contrast to the rather involved expressions given there for a one-component plasma, here we could restrict the potential energy sum only by the proper sum in *real space* (we do not reproduce these lengthy expressions here, but mention that the value of the parameter β defined in Ref. [22] was chosen to be $\beta = 5.6/L$) and taking 5 vectors in every direction in *the reciprocal space*. This gives some computational-cost advantage in computation of the forces compared to Ref. [22].

In Fig. 8, we plot the internal energy per atom as a function of temperature for two densities and compare it to the path integral Monte Carlo results of Militzer [41]. One can note, that for high temperatures the energies of MD and PIMC simulations coincide very well and lie within the limits of the statistical errors. This is an important test for the simulation, and this agreement was expected due to the asymptotic character of the Kelbg potential as a rigorous weak coupling result. Moreover, we observe practically full agreement between MD and PIMC results to temperature as low as approximately 50 000K, corresponding to a coupling parameter $\beta = 3$. This is a remarkable extension of “semiclassical” molecular dynamics into the regime of moderate coupling and moderate degeneracy.

Naturally, below a critical temperature of about 50 000 K deviations from PIMC results start to grow rapidly – the MD results for the energy are becoming very low. It is very interesting to analyze the reasons for these deviations, as this may suggest directions for further improvements. It turns out that the reason for these deviations is not a failure of the used quantum pair potentials. Thus the only source for the deviations in the full simulation can be many-particle effects beyond the two-particle level.

To verify this hypothesis we performed a careful inspection of the microscopic particle configurations in the simulation box. At high temperatures, the particle trajectories are those of a fully ionized classical plasma. At temperatures below on Ry, we observe an increasing number of electrons undergoing strong deflections on protons and eventually performing quasibound trajectories. Most of these electrons remain “bound” only for a few classical orbits and then leave the proton again. Averaged over a long time our simulations are able to reveal the degree of ionization of the plasma. At the same time we observe occasional events of three and more particles being at short distances for the duration of one or more orbits, reflecting the appearance of hydrogen molecules H_2 , molecular ions H_2^+ etc.

If the temperature is lowered below approximately $T = 50\,000$ K, we observe a strong increase of molecule formation and even an aggregation of many molecules into clusters with an interparticle distance close to one a_B . This turns out to be the reason for the observed very low energy because the attractive Coulomb interaction contributions are becoming dominant in the total energy. Of course, this behavior is not surprising: while all pair interaction processes are modelled correctly even

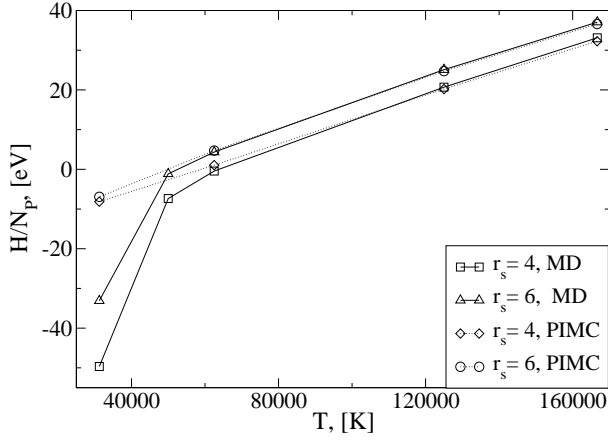


Figure 8: Semiclassical MD results (full lines) for the internal energy per hydrogen atom at densities $r_s = 4, 6$ versus temperature. The results of restricted PIMC simulations by Militzer [41] are shown for comparison (dashed lines). Symbols indicate the five temperatures for which MD simulations have been performed: $T = 31\,250, 50\,000, 62\,500, 125\,000$ and $166\,670$ K (solid lines). The pair approximation breaks down around $50\,000$ K, at the molecule binding energy.

at low temperature (which is assured by the fit parameters in the improved Kelbg potentials), as soon as three or more particles are being closely together, three-particle and higher order correlations are becoming increasingly strong (they, in particular, account for the formation of the larger bound state complexes described above). However, it was just the approximation used in the derivation of the quantum potentials that three-particle and higher correlations can be neglected which was the basis for the use of pair potentials in modelling the whole N -particle system. While molecular dynamics, of course, includes any level of correlations, the use of the present potentials means that *quantum corrections to three-body (and higher order) interactions* are not adequately captured. Therefore, it is no surprise that this approximation breaks down at sufficiently low temperature, and this break down occurs around the temperature corresponding to the binding energy of hydrogen molecules. From this we can conclude that molecule formation sets the limit of the applicability of the present semiclassical MD simulations.

Let us now turn to a more detailed analysis of the spatial configuration of the particles in the MD simulations.

In Fig. 9 the radial pair distributions between all particle species with the same charge are plotted at two densities. Consider first the case of $T = 125\,000$ K (upper panel). For both densities, all functions look qualitatively the same, showing a depletion at zero distance due to Coulomb repulsion. Besides, there are differences which arise from the spin properties. Electrons with same spin show a slightly broader “Coulomb hole” around $r = 0$ than the protons, because the Pauli principle yields an additional repulsion of the electrons (this effect is much

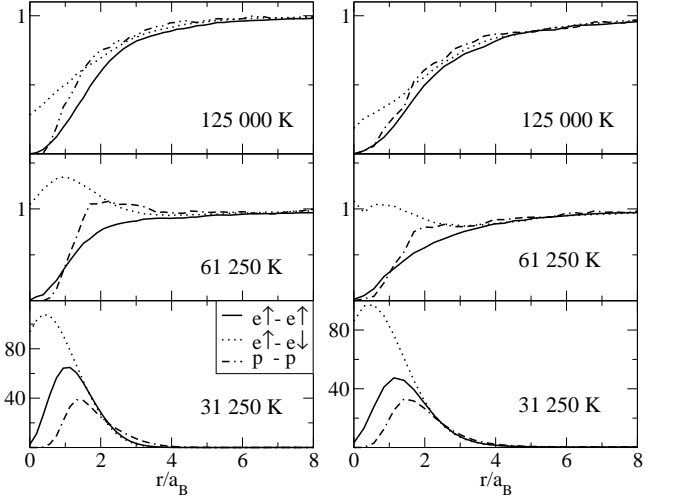


Figure 9: Electron-electron and proton-proton radial pair distribution functions for a correlated hydrogen plasma with $r_s = 4$ (left row) and $r_s = 6$ (right row) for $T = 125\,000; 61\,250$ and $31\,250$ K (from top to bottom).

weaker for two protons due to their much smaller de Broglie wavelength). This trend is reversed at lower temperature, see middle panel, which is due to the formation of hydrogen atoms, see also Fig. 11 below. In this case, electrons (their trajectories) are “spread out” around the protons giving rise to an increased probability of close encounters of two electrons in different atoms compared to two protons.

Now, let us compare electrons with parallel vs. electrons with antiparallel spins. In all cases, we observe a significantly increased probability to find two electrons with opposite spin and small distances below one Bohr radius which is due to the missing Pauli repulsion in this case. This trend increases with lowering of temperature due to increasing quantum effects and thus convincingly confirms that spin effects are correctly reproduced in our MD simulations.

Before analyzing the lowest temperature in Fig. 9 let us consider the electron-proton pair distributions which are shown in Fig. 10. With lowering of temperature, we observe a strong increase of the probability to find an electron close to a proton. In contrast to the classical case of a collapse (see above), here this probability is finite. Multiplying these functions by r^2 gives essentially the radial probability which is plotted in Fig. 11. Here, lowering of temperature leads towards formation of shoulder around $1.5a_B$ which is due to the formation of hydrogen atoms. This conclusion is confirmed by inspection of the corresponding quasibound electron trajectories as discussed above. At this temperature, the observed most probable electron distance is not $1a_B$ as in the hydrogen ground state which is due to the considerable kinetic energy of the particles leading to a larger average radius of the classical quasiclosed orbits. We expect that at lower

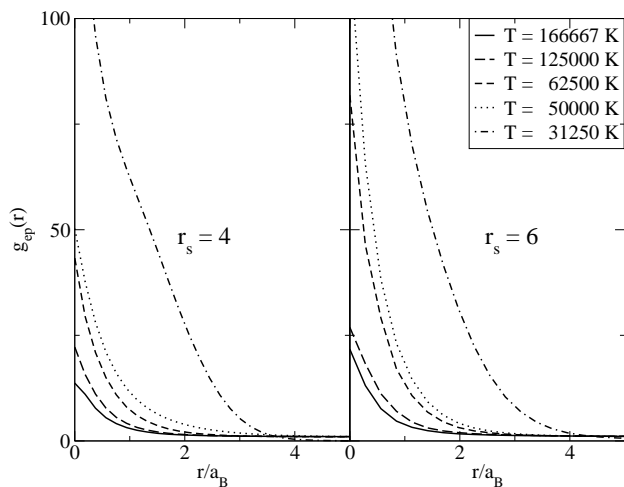


Figure 10: Electron-proton radial pair distribution functions at $r_s=4$ (left figure) and $r_s=6$ (right figure) and five temperatures: $T = 166\,667; 125\,000; 62\,500$ and $50\,000$ K.

temperature, the most probable radius would tend towards $1a_B$, but this temperature range is not realistically modelled due to molecule and cluster formation.

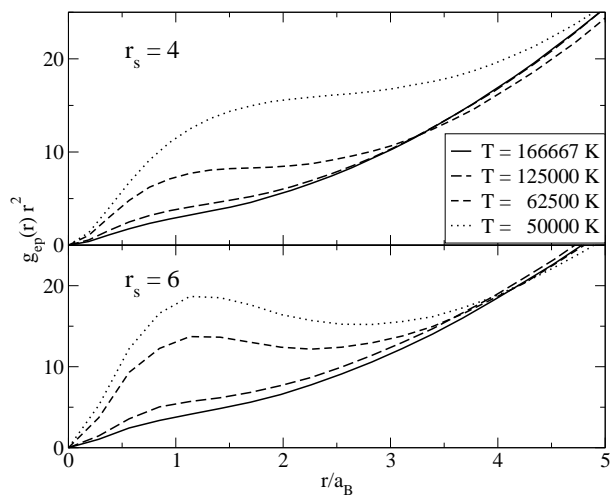


Figure 11: Electron-proton radial pair distribution functions multiplied by r^2 . Same data as in Fig. 10.

While the description of correlated complexes of more than two particles is certainly beyond the present pair approximation model, nevertheless, several features of a partially ionized and partially dissociated hydrogen plasma are reproduced correctly. At $62\,500$ K and $r_s = 6$ (right center part of Fig. 9) the simulations show a first weak signature of molecule formation – see the maximum of the p-p pair distribution function around $r = 2a_B$ and the maximum of the pair distribution function of electrons with antiparallel spins around $r = 1.5a_B$. Further lowering of the temperature by a factor of two (lower panel of Fig. 9) confirms this trend: the p-p functions exhibit a clear peak very close to $r = 1.4a_B$ – the theo-

retical p-p separation in H_2 -molecules. At the same time, also the e-e functions have a clear peak around $r = 0.5a_B$, in the case of opposite spins, and $r = 1.2a_B$, for parallel spin projections. The first case comes rather close to the true quantum mechanical $H-H$ bound state (singlet) with the electron wave function predominantly concentrated between the two protons. On the other hand, this electron peak should also extend to the right of the p-p peak, and no such pronounced peak would be expected for electrons with the same spin.

Nevertheless, we may conclude that even formation and spatial dimension of hydrogen molecules appear to be captured surprisingly well in these simulations. The main difficulty appears to arise not on the level of four-particle correlations but on the level of six particle correlations: in the simulations nothing prevents two “bound” atoms from binding to a third and more atoms. The overall attractive Coulomb interaction makes it, below $50\,000$ K, energetically favorable to form large clusters consisting of more than two atoms, explaining the strong decrease of the internal energy at the $T = 31\,250$ K, cf. Fig. 8. In reality, complexes of two molecules do exist, but they have a very low binding energy which is due to a subtle compensation effects arising from repulsive exchange interaction between the electrons which go far beyond the level of pair interactions [42].

VI. USE OF THE QUANTUM PAIR POTENTIALS IN DENSITY FUNCTIONAL THEORY

The effective quantum potentials have been introduced to represent the equilibrium two particle density matrix and subsequently generalized to incorporate many-body Coulomb coupling effects. There are other many body coupling effects due to degeneracy or exchange correlations. For some applications, it may be useful to incorporate these directly in the effective pair potentials to extend their validity to still lower temperatures, as was demonstrated on the example of classical MD above.

In this section, we describe the usefulness of the effective quantum potentials for a completely different theoretical approach – density functional theory (DFT). In doing so, the role of effective quantum potentials with degeneracy effects is illustrated as well.

DFT is a formal structure in which non-perturbative approximations can be introduced to describe strong coupling effects [43]. Although there are both classical and quantum versions of DFT, the classical form does not apply to a system of electrons and positive ions due to the Coulomb divergence. One possibility is to postulate a classical statistical mechanics using the effective quantum potentials described above which allows to remove the singularity. Alternatively, the proper quantum formulation can be used from the outset and the effective quantum potentials “derived” as a tool in the process of computing properties of interest [44]. This second ap-

proach will be used here.

In essence, DFT is a variational means to derive an equation for the charge density induced by an external potential. If that potential is taken to be the same as the potential of one of the charges in the system, the resulting density is in fact formally identical to the equilibrium pair correlation function, or diagonal element of the two particle density matrix. The density obeys a known nonlinear integral equation – a generalization of the Boltzmann-Poisson equation. However, in practice, the direct solution this equation is seldom attempted. Instead an equivalent set of self-consistent one particle Schrödinger equations, the Kohn-Sham equations [45], are solved first to construct the charge density. Yet it might be very useful to recall the existence of an alternative direct approach which becomes practical if an appropriate quantum pair potential is introduced. This is illustrated in more detail as follows.

Consider a quantum system in the presence of external sources that can be described by an additive potential

$$\hat{\psi} = \sum_{i=1}^X \hat{\psi}(\mathbf{q}_i): \quad (41)$$

Here $\hat{\psi}$ denotes a species and \mathbf{q}_i is the position operator of particle i of species ψ . The caret on the potentials is used to distinguish the quantum operator from its corresponding function. In general, each species may have a different form for the coupling to the external sources. The potential also can be written in terms of the density operators for each species

$$\hat{\psi} = \sum_{\mathbf{r}} \sum_{\mathbf{r}'} \sum_{i=1}^X V(\mathbf{r}) \hat{\mathbf{b}}(\mathbf{r}); \quad \hat{\mathbf{b}}(\mathbf{r}) = \sum_{i=1}^X (\mathbf{r} | \mathbf{q}_i): \quad (42)$$

The details of the remainder of the Hamiltonian are not important at this point. For this many-body system with external sources the theorems of density functional theory apply in the following form. First, a functional of the average densities, $\mathbf{b}(\mathbf{r})$, averaged over an equilibrium grand canonical ensemble is constructed (the generalization to other equilibrium ensembles has been carried out). This is done in two steps. First, the equilibrium grand potential for the system is considered formally

$$\Omega_e = - \ln \sum_{\{f_n, g\}} \text{Tre} \left(e^{-\beta H} \right): \quad (43)$$

The density for the various species is obtained (formally) by functional differentiation with respect to the potentials

$$n_e = - \frac{\delta \Omega_e}{\delta V(\mathbf{r})}; \quad n_e(\mathbf{r}) = \frac{\delta \Omega_e}{\delta V(\mathbf{r})}: \quad (44)$$

The density equation is inverted (formally) to get the external potentials as functionals of the average densities

$$V = V(\mathbf{r} | f n_e, g); \quad (45)$$

and a Legendre transformation is performed to construct the free energy as a functional of the densities rather than the chemical potentials

$$F(f n_e, g) = \sum_{\mathbf{r}} \left(\frac{f}{2} V(\mathbf{r}) g \right) + \sum_{\mathbf{r}} \text{dr} [V(\mathbf{r} | f n_e, g)] n_e(\mathbf{r}): \quad (46)$$

The crucial second step is to extend this functional to *arbitrary density fields*

$$F(f n_e, g) \rightarrow F(f n, g): \quad (47)$$

The main task of density functional theory is now to construct the density functional

$$\Omega_v(f n, g) = F(f n, g) - \sum_{\mathbf{r}} \text{dr} (V(\mathbf{r})) n(\mathbf{r}); \quad (48)$$

where, in this definition, $V(\mathbf{r})$ is *not* considered to be a functional of the density. The main theorem of density functional theory is then that this functional has an extremum at the equilibrium density

$$\frac{\delta \Omega_v(f n, g)}{\delta n} = 0 = \frac{\delta F(f n, g)}{\delta n} [V(\mathbf{r})]; \quad (49)$$

Furthermore the value of the functional at the equilibrium density is clearly the equilibrium grand potential

$$\Omega_v(f n, g) = \Omega_e(f n_e, g):$$

In practice, an approximate free energy functional $F(f n, g)$ is written and Eq. (49) is solved to obtain the equilibrium density. This density is then used to evaluate the equilibrium grand potential and determine all equilibrium thermodynamic properties. Structural properties can be obtained as well by choosing the external potential at the end to be the same as that for interaction among the system particles. In other words, the source is chosen to be a particle of the same type as those comprising the many-body system. The densities n_e become equilibrium pair correlation functions.

How should the functional $F(f n, g)$ be constructed? There is clearly a part associated with an ideal gas, and an energy due to the direct Coulomb interactions. These can be identified explicitly. In addition there are the more difficult parts due to exchange and correlations. Consequently, it has become standard practice to write the free energy as

$$F[n] = F^{(0)}(f n, g) + \frac{1}{2} \sum_{\mathbf{r}} \sum_{\mathbf{r}'} \text{dr dr}' V(\mathbf{r} - \mathbf{r}') n(\mathbf{r}) n(\mathbf{r}') + F_{xc}(f n, g); \quad (50)$$

where $F^{(0)}(f n, g)$ is the free energy for the non-interacting system, the second term is the contribution from the direct Coulomb interaction, and $F_{xc}(f n, g)$ denotes the remaining contributions due to interactions from exchange

and correlations. Then the extremum condition (49) becomes [44]

$$\frac{\delta V^{(0)}(\mathbf{r}; \mathbf{j} \mathbf{n})}{\delta \mathbf{r}} = \frac{\delta V(\mathbf{r})}{\delta \mathbf{r}} + \frac{F_{xc}(\mathbf{r})}{n(\mathbf{r})}; \quad (51)$$

with $V^{(0)}(\mathbf{r}; \mathbf{j} \mathbf{n})$ denoting the functional (45) for the ideal gas. Determination of this functional is the central issue of the discussion here, and we will show that it is closely related to the Kelbg potential analyzed in the bulk of this paper.

The definition of the functional $V^{(0)}(\mathbf{r}; \mathbf{j} \mathbf{n})$ is straightforward from the representation of the density for an *ideal Fermi gas* in the external potentials

$$n(\mathbf{r}) = \int \frac{d^3p}{(2\pi)^3} e^{-\beta \left(\frac{p^2}{2m} + \Phi(\mathbf{r}) \right)} + 1^{-1} \quad (52)$$

This is a single particle problem. The right side is clearly a functional of V through the dependence of the eigenvalues of $\frac{p^2}{2m} + \Phi$ on the form of the external potential. Interestingly, even at the level of the ideal gas determination of this functional is non-trivial. In the *non-degenerate limit* this equation for the density becomes

$$n(\mathbf{r}) \approx \int \frac{d^3p}{(2\pi)^3} e^{-\beta \left(\frac{p^2}{2m} + \Phi(\mathbf{r}) \right)} \quad (53)$$

If the external potential is chosen to be a Coulomb source, then (53) becomes equivalent to the diagonal elements of the two particle density matrix in relative coordinates which has exactly the form of the pair distribution function used to define the effective quantum pair potential, cf. Eq. (27).

Once the exchange and correlation free energy functional is specified (guessed), (51) provides a set of closed *classical* integral equations for the equilibrium densities. As will be seen below, a leading approximation is the usual Boltzmann-Poisson representation in terms of semi-classical potentials. The primary technical difficulty in this prescription is the determination of $V^{(0)}(\mathbf{r}; \mathbf{j} \mathbf{n})$. Kohn and Sham noted that (51) defines an effective single particle potential and therefore is formally equivalent to the ideal gas in this effective potential. Therefore, the solution can be constructed by solving the one particle Schrödinger equation whose potential is the right side of (51), and calculating the densities from the associated form (52) self-consistently

$$n(\mathbf{r}) = \int \frac{d^3p}{(2\pi)^3} e^{-\beta \left(\frac{p^2}{2m} + \Phi(\mathbf{r}) \right)} + 1^{-1} \quad (54)$$

This avoids the difficult problem of finding the functional $V^{(0)}(\mathbf{r}; \mathbf{j} \mathbf{n})$ but at the cost of having to solve a set of self-consistent Schrödinger equations.

Consider instead an approximate evaluation of the potential $V^{(0)}(\mathbf{r}; \mathbf{j} \mathbf{n})$ in terms of an effective quantum potential $U(\mathbf{r})$ defined by

$$n(\mathbf{r}) = \int \frac{d^3p}{(2\pi)^3} e^{-\beta \left(\frac{p^2}{2m} + U(\mathbf{r}) \right)} + 1^{-1} \quad (55)$$

The first equality is similar to a finite temperature Thomas-Fermi representation, with a local chemical potential given by $\mu(\mathbf{r}) = U(\mathbf{r})$. An important difference discussed below is that $U(\mathbf{r}) \neq V(\mathbf{r})$. The functional relationship of $n(\mathbf{r})$ to $U(\mathbf{r})$ and hence to $V(\mathbf{r})$ is that for an ideal gas and is well-known. The second equality of (55) defines the semi-classical potential $U(\mathbf{r}; V^{(0)})$ as a functional of $V^{(0)}$. This relationship of $U(\mathbf{r}; V^{(0)})$ to $V^{(0)}$ is more difficult to unfold. However, it is straightforward to discover it for weak coupling of the system to the perturbing potential. The analysis is similar to the derivation of the Kelbg potential and will not be repeated here. Formally make the replacement $\Phi^{(0)} \rightarrow \Phi^{(0)}$ in (55) with the corresponding dependence on $V^{(0)}$ inherited by $U(\mathbf{r})$. Then perform the expansion of $U(\mathbf{r})$ to first order in $V^{(0)}$, setting $\beta = 1$ at the end, to get [44]

$$U(\mathbf{r}) \approx \int d^3r^0 (\mathbf{r} - \mathbf{r}^0) V^{(0)}(\mathbf{r}^0) \quad (56)$$

where $(\mathbf{r}; \mathbf{r}^0)$ is the well-known static linear polarization function in random phase approximation,

$$(\mathbf{r}) = \int \frac{d^3p}{(2\pi)^3} e^{i\mathbf{k} \cdot \mathbf{r}} e^{-\beta \left(\frac{p^2}{2m} + \Phi(\mathbf{r}) \right)} \quad (57)$$

$$e^{-\beta \left(\frac{p^2}{2m} + \Phi(\mathbf{r}) \right)} = \frac{1}{n} \int \frac{d^3p}{(2\pi)^3} \frac{F(p)}{p^2} \frac{F(p)}{(\mathbf{p} - \mathbf{k})^2}; \quad (58)$$

containing the Fermi distribution

$$F(p) = \int \frac{d^3p}{(2\pi)^3} e^{-\beta \left(\frac{p^2}{2m} + \Phi(\mathbf{r}) \right)} + 1^{-1} \quad (59)$$

In this approximation, the functional relationship between the density and the potential is now known

$$n(\mathbf{r}) = \int \frac{d^3p}{(2\pi)^3} e^{-\beta \left(\frac{p^2}{2m} + \int d^3r^0 (\mathbf{r} - \mathbf{r}^0) V^{(0)}(\mathbf{r}^0) \right)} + 1^{-1} \quad (60)$$

Now it is straightforward to improve this results by substitution of (51) into the right side of (60) which gives a generalization of the Thomas-Fermi approximation to include strong coupling effects. However, even if $F_{xc}(\mathbf{r})$ is neglected the result is the Thomas-Fermi approximation in terms of the potential

$$\bar{V}(\mathbf{r}) = \int d^3r^0 (\mathbf{r} - \mathbf{r}^0) V(\mathbf{r}^0) \quad (61)$$

rather than the bare potential $V(\mathbf{r})$, which has short ranged divergences for opposite charge interactions. The result here in terms of the *nonlocal effective quantum potential* appears to be a new one that cures some of the well-known problems of the “local approximation” Thomas-Fermi theory. As indicated below, $\bar{V}(\mathbf{r})$ becomes just the Kelbg potential in the non-degenerate limit. The result (60) with (51) is a non-linear integral equation for the density, including both *strong coupling and degeneracy effects*. There is no longer any need to solve the Kohn-Sham equations and the problem is one of purely classical analysis.

It is instructive to consider the non-degenerate limit. In that case the polarization function is evaluated using $F_0(\mathbf{p}) \approx e^{-\frac{p^2}{2m}}$. Furthermore, Eq. (60) simplifies to

$$n(\mathbf{r}) = \frac{n}{Z} e^{-U(\mathbf{r})}; \quad (62)$$

$$V^{(0)}(\mathbf{r}^0) = \int d\mathbf{r}^0 \frac{1}{|\mathbf{r} - \mathbf{r}^0|} U(\mathbf{r}^0); \quad (63)$$

Use of these in the DFT equation (51) gives the closed equation for the densities

$$\ln \frac{n(\mathbf{r})}{n} = -\frac{1}{n} \int d\mathbf{r}^0 \bar{V}(\mathbf{r} - \mathbf{r}^0) n(\mathbf{r}^0) + \int d\mathbf{r}^0 \frac{F_{xc}(\mathbf{r} - \mathbf{r}^0)}{n(\mathbf{r}^0)}; \quad (64)$$

The potentials $\bar{V}(\mathbf{r})$ and $\bar{V}(\mathbf{r} - \mathbf{r}^0)$ are “regularized” by the polarization function, e.g.,

$$\bar{V}(\mathbf{r}) = \int d\mathbf{r}^0 \frac{1}{|\mathbf{r} - \mathbf{r}^0|} V(\mathbf{r}^0); \quad (65)$$

It is possible to show [46] that in this *non-degenerate limit* $\bar{V}(\mathbf{r})$ is just the original Kelbg potential, Eq. (4). Therefore, in the weak coupling limit where $F_{xc}(\mathbf{r})$ can be neglected (64) becomes the usual Boltzmann-Poisson equation with effective quantum potentials given by the Kelbg potential (4).

In summary, DFT applications can be performed in a semi-classical form without solving the Kohn-Sham equations by introducing effective quantum potentials. This can be done in a weak coupling approximation similar to that first described by Kelbg and yields a closed analytical result (4). Based on the results of the above analysis, it can be expected that this approach can be extended by incorporating as well effects of degeneracy by using for the density Eq. (52) instead of (62). Furthermore by using *improved quantum pair potentials* – along the lines of the improved Kelbg potentials discussed in the previous sections – an accurate treatment of the pair problem is achieved laying the foundation for advancing DFT to the regime of strong coupling.

VII. CONCLUSION

In this work we presented an analysis of generalized quantum pair potentials. Extending the work of Kelbg and others we investigated in detail *effective off-diagonal and diagonal quantum pair potentials* for a correlated hydrogen plasma including spin effects. We studied the accuracy of these potentials by an extensive comparison with the exact solutions of the Bloch equation. Further, we proceeded to an analysis of *improved diagonal quantum pair potentials* by correcting the value of the Kelbg potential at zero particle separation. Excellent agreement with the exact solutions of the two-particle Bloch equations could be achieved with the help of a single temperature-dependent fit parameter for which an accurate analytical Padé formula was presented. This led to significantly improved diagonal pair potentials compared to the original Kelbg potential. Moreover, these potentials are explicitly spin-dependent and retain the advantage of a closed analytical expression.

These potentials have been applied in path integral Monte Carlo and “semiclassical” molecular dynamics simulations of dense hydrogen and were found to give accurate results over a wide range of parameters. One important conclusion, of relevance to PIMC simulations, is that the off-diagonal potential gives essentially more accurate results (or more rapid convergence) than its diagonal limit, quantitative estimates have been provided.

Furthermore, we have demonstrated that the spin-dependent improved diagonal potentials are of high use for “semiclassical” molecular dynamics simulations of partially ionized plasmas. Our analysis revealed that with these potentials one can successfully simulate dense hydrogen up to moderate coupling and degeneracy, from the fully ionized to the partially ionized regime. The present potentials allow us to correctly model dense plasmas up to temperatures as low as the molecular binding energy. Further improvements are possible, including the description of molecular hydrogen, but they require to include three-particle and four-particle correlations and exchange effects beyond the two-particle level.

Finally an intimate relation of the quantum potentials to density functional theory has been explored which allows for DFT calculations without the need to solve the Kohn-Sham equations.

VIII. ACKNOWLEDGMENTS

We acknowledge stimulating discussions with V. Filinov, W.D. Kraeft, D. Kremp and M. Schlanges. M.B. gratefully acknowledges hospitality of the Physics Department of the University of Florida.

This work has been supported by the Deutsche Forschungsgemeinschaft (BO-1366/2), the National Science Foundation and the Department of Energy (grants DE FG03-98DP00218 and DE FG02ER54677), as well as by grants for CPU time at the NIC Jülich and the

-
- [1] A. Filinov, M. Bonitz, and W. Ebeling, J. Phys. A: Math.Gen. **36**, 5957 (2003).
- [2] *Strongly Coupled Coulomb Systems*, G. Kalman (ed.), Pergamon Press 1998.
- [3] *Proceedings of the International Conference on Strongly Coupled Plasmas*, W.D. Kraeft and M. Schlanges (eds.), World Scientific, Singapore 1996.
- [4] W.D. Kraeft, D. Kremp, W. Ebeling, and G. Röpke, *Quantum Statistics of Charged Particle Systems*, Akademie-Verlag Berlin 1986.
- [5] M. Bonitz, “Quantum Kinetic Theory”, B.G. Teubner, Stuttgart/Leipzig 1998.
- [6] H. Haberland, M. Schlanges, W. Ebeling (eds.): Proc. 10th Int. Workshop on the Physics of Nonideal Plasmas, Contrib. Plasma Phys. **41**, No 2-3 (2001).
- [7] “*Progress in Nonequilibrium Greens Functions*”, M. Bonitz (ed.), World Scientific Publ., Singapore 2000.
- [8] L.B. Da Silva et al., Phys. Rev. Lett. **78**, 483 (1997).
- [9] S.T. Weir, A.C. Mitchell, and W.J. Nellis, Phys. Rev. Lett. **76**, 1860 (1996).
- [10] G.E. Norman, and A.N. Starostin, Teplofiz. Vys. Temp. **6**, 410 (1968); **8**, 413 (1970), [Sov. Phys. High Temp. **6**, 394 (1968); **8**, 381 (1970)]
- [11] P. Haronska, D. Kremp, and M. Schlanges, Wiss. Z. Universität Rostock **98**, 1 (1987).
- [12] D. Saumon, and G. Chabrier, Phys. Rev. A **44**, 5122 (1991).
- [13] M. Schlanges, M. Bonitz, and A. Tschttschjan, Contrib. Plasma Phys. **35**, 109 (1995).
- [14] D. Beule et al., Phys. Rev. B **59**, 14177 (1999); Contrib. Plasma Phys. **39**, 21 (1999)
- [15] V.S. Filinov, V.E. Fortov, M. Bonitz, and P.R. Levashov, JETP Lett. **74**, 384 (2001) [Pis'ma v ZhETF **74**, 422 (2001)].
- [16] W. Ebeling, W.D. Kraeft, and D. Kremp, “Theory of bound states and ionization equilibrium in plasmas and solids”. Akademie-Verlag Berlin 1976; Russ. Transl. Mir Moscow 1979.
- [17] W.R. Magro, D.M. Ceperley, C. Pierleoni and B. Bernu, Phys. Rev. Lett. **76**, 1240 (1996).
- [18] B. Militzer and D.M. Ceperley, Phys. Rev. E **63**, 066404 (2001).
- [19] S.A. Trigger, W. Ebeling, V.S. Filinov, V.E. Fortov, M. Bonitz, JETP **96**, 465 (2003).
- [20] V.S. Filinov, M. Bonitz, W. Ebeling, and V.E. Fortov, Plasma Physics and Controlled Fusion **43**, 743 (2001).
- [21] D. Klakow, C. Toepffer, and P.-G. Reinhard, Phys. Lett. A **192**, 55 (1994); J. Chem. Phys. **101**, 10766 (1994).
- [22] V. Golubnychiy, M. Bonitz, D. Kremp, and M. Schlanges, Phys. Rev. E **64**, 016409 (2001).
- [23] For completeness we mention interesting concepts of quantum MD, such as wave packet MD, e.g. [21] and Wigner function MD [24], which are, however, beyond the scope of this paper.
- [24] V.S. Filinov, P. Thomas, I. Varga, T. Meier, M. Bonitz, V.E. Fortov, and S.W. Koch, Phys. Rev. B **65**, 165124 (2002).
- [25] G. Kelbg, Ann. Physik, **12**, 219 (1963); **13**, 354; **14**, 394 (1964).
- [26] C. Deutsch, Phys. Lett. **60A**, 317 (1977).
- [27] F.J. Rogers, Phys. Rev. A **23**, 1008 (1981).
- [28] M.-M. Gombert, H. Minoo, and C. Deutsch, Phys. Rev. A **29**, 940 (1984).
- [29] F. Perrot and M.W.C. Dharma-wardana, Phys. Rev. B **62**, 16536 (2000).
- [30] M.-M. Gombert, H. Minoo, Contrib. Plasma Phys. **29**, 355 (1989).
- [31] H. Wagenknecht, W. Ebeling, and A. Förster, Contrib. Plasma Phys. **41**, 15 (2001).
- [32] R.G. Storer, J. Math. Phys. **9**, 964 (1968); A.D. Klemm, and R.G. Storer, Aust. J. Phys. **26**, 43 (1973).
- [33] A.A. Barker, J. Chem. Phys. **55**, 1751 (1971).
- [34] B. Davies and R.G. Storer, Phys. Rev. **171**, 150 (1968).
- [35] K. Rodhe, G. Kelbg, and W. Ebeling, Ann. Phys. **22**, 1 (1968).
- [36] M.-M. Gombert, Phys. Rev. E **66**, 066407 (2002).
- [37] D.M. Ceperley, Rev. Mod. Phys. **65**, 279 (1995).
- [38] H. Kleinert, *Path Integrals in Quantum Mechanics, Statistics and Polymer Physics*, World Scientific, Second edition, 1995.
- [39] H. Kleinert, Phys. Rev. D **57**, 2264 (1998).
- [40] Since, in this case, individual electrons do not change their spin projection, no exchange processes during collisions occur. This allows us to treat the electrons with opposite spin projection as distinguishable particles and to neglect exchange contributions to the pair potentials. In contrast, in the scattering of two electrons with the same spin projection exchange does take place which is taken into account by the potential (14). For a discussion of this question, see C. Cohen-Tannoudji, B. Diu, and F. Laloe, *Quantum Mechanics, vol. 2*, Ch. 14, John Wiley & Sons 1977.
- [41] B. Militzer, PhD thesis, University Illinois, (2000).
- [42] More details of the MD simulations are given in V. Golubnychiy, PhD thesis, Rostock University 2004.
- [43] N.D Mermin, Phys. Rev. **137**, A1441 (1965).
- [44] L. Zogaib and J. Dufty (to be published).
- [45] W. Kohn and L. Sham, Phys. Rev. **140**, A1133 (1965).
- [46] J.W. Dufty, unpublished.